Fall 2018

Conical folds -- An artifact of using simple geometric shapes to describe a complex geologic structure

Avery Joseph Welker

Department:

CONICAL FOLDS - AN ARTIFACT OF USING SIMPLE GEOMETRIC SHAPES TO DESCRIBE A COMPLEX GEOLOGIC STRUCTURE

by

AVERY JOSEPH WELKER

A THESIS

Presented to the Graduate Faculty of the

MISSOURI UNIVERSITY OF SCIENCE AND TECHNOLOGY

In Partial Fulfillment of the Requirements for the Degree

MASTER OF SCIENCE

in

PETROLEUM ENGINEERING

2018

Approved by

Andreas Eckert, Advisor
John P. Hogan
Jonathan Obrist-Farner

ABSTRACT

Accurate representation of the 3D shapes of natural folds is essential to characterization of the dynamic models for fold formation. Geometrical analysis of folds commonly relies upon analyzing patterns defined by the variation in the orientation of poles to planar surfaces deformed by a shortening event when plotted using graphical calculators (e.g., stereogram, polar tangent diagrams) to interpret the shape of folds. Stereograms for which orientation data define small circles are classified as non-cylindrical regular folds and are interpreted as "conical folds," where the shape of the fold is represented by a cone that terminates at a point. Utilizing similar two-dimensional geometrical analysis of orientation data extracted from various transects across virtual pericline folds produces high spatial resolution synthetic stereograms with patterns that reproduce those of cylindrical and non-cylindrical conical folds as well as "fish-hook" patterns. Stereograms from natural periclines near Licking, Missouri mimic those of the synthetic stereogram patterns. Reverse engineering to produce three-dimensional shapes from the synthetic stereogram defines cones as this is a permissible solution to this stereogram pattern; however, the shape and orientation of these cones are shown to be poor representations of the shape of the pericline. Additionally, SCAT and differential geometry analyses are used to mathematically demonstrate the difference between periclines and conical folds. In comparison to conical folds, natural pericline folds are common, and their formation is readily reproduced by dynamic modelling without requiring highly non-uniform stress-fields or special mechanical behavior. We suggest that continuing to model the geometrical shape of many natural folds as conical, based upon stereogram patterns that define small circles, is pointless as natural folded rocks are more likely to have the form of periclines.

ACKNOWLEDGMENTS

I would like to thank my advisor, Dr. Andreas Eckert, for helping me navigate my journey into graduate school, through my master's degree, and as I go forward into my Ph.D. Accepting me into the Geomechanics Task Force has given me a monumentally valuable developmental experience. Throughout my time as an undergraduate, when he was also my advisor, he was supportive and helpful with guiding me and helping me hone my technical and communicative skills, which will carry me far in life. I would also like to thank Dr. John P. Hogan for the incalculable time and effort he has put into this thesis and the resulting paper. Our goals for this thesis have been lofty. Through our collaboration and teamwork, we have put together an impactful paper. His conversation is always stimulating, and very thought-provoking. Thanks to Dr. Jonathan Obrist-Farner and to my committee as a whole. Managing my constantly-evolving project has been a difficult process, but I am glad that we have gone through it.

Many thanks go out to my colleagues-turned-friends who are in (or were) part of the Geomechanics Task Force: William Chandonia, Chao Liu, Weicheng Zhang, Yuxing Wu, Jianbo Liu, Xiaolong Liu, Eli Steinbeck, Wenyu Zhao, Peter Nso, and Qiaoqi Sun. I deeply appreciate the collaborative environment we have worked hard to create, open flow of information between all of us, and your friendship.

Lastly, I would like to thank my family and friends: my parents Kenneth and Tammie Welker, my sister Lydia Welker, and all of my friends (too many to count). Thanks for your support and encouragement through these past couple of years. It's been quite a ride. Thank you for keeping me sane!

The authors acknowledge the use of the Move Software Suite granted by Midland Valley's Academic Software Initiative. Helpful suggestions on an early version of this manuscript by Michael Williams are greatly appreciated.

TABLE OF CONTENTS

Page

LIST OF ILLUSTRATIONS

NOMENCLATURE

Symbol	Description
λ	Wavelength
A	Fold Amplitude
W	Fold Width

1. INTRODUCTION

1.1. OVERVIEW AND MOTIVATION

Understanding fold formation, where rock layers buckle or bend without necessarily breaking, continues to attract the attention of many geologists. Dynamic models of folding (e.g., Biot *et al.* (1961); Ramberg (1963); Hudleston and Lan (1993); Hudleston and Lan (1994); Schmalholz and Podladchikov (2001); Liu *et al.* (2016)) receive favorable consideration based upon how faithfully they reproduce the geometric form of folded rock surfaces. Consequently, geometric analysis of fold shapes must faithfully represent the true geometry of folded surfaces, which can be challenging, especially at the terminus of folds.

1.1.1. Fold Classification. Geologists typically characterize fold shapes through measurement of geometric elements of folds such as the axial surface, hinge-line, crest-line, inter-limb angle, amplitude, width, and wavelength (e.g., Dahlstrom (1954); Wilson (1967); Ramsay (1967); Hudleston and Treagus (2010)). For well-exposed folds, several geometric elements can be measured in the field. More commonly, large portions of folds, including fold terminuses, are poorly exposed and geologists use orientation data from available exposures and graphical calculators (e.g., stereonets, tangent diagrams) to characterize fold geometries (e.g., Davis *et al.* (2011)). Using stereonets, fold shapes are classified as cylindrical, near-cylindrical, or non-cylindrical based upon a statistical fit of poles to the folded surface(s) to a great circle – the π-circle. Treating folds as cylindrical or near-cylindrical, where the fold shape remains constant along the entirety of the hinge line, allows for quantitative description of geometric elements of folded surfaces and further classification of the fold (e.g., Fleuty (1964); Ramsay (1967); Hudleston (1973)). This

information is of considerable use in the construction of geologic maps, cross-sections, as well as exploration of natural resources such as subsurface petroleum reservoirs (e.g., Groshong, Jr. (2006)).

1.1.2. Fold Terminations. The ability to use graphical calculators for constraining structural elements, even with sparse data sets, is a rite of passage for many if not all geology students, and many folds or portions of folds are tacitly treated as being cylindrical or near-cylindrical. However, Wilson (1967) warns, "*No fold, cylindrical or otherwise, can continue indefinitely – somewhere or other it will die out.*" Thus, even cylindrical folds eventually transition to non-cylindrical folds towards the fold terminus. Accurately characterizing the changes in fold geometry towards the fold terminus is important to understanding fold forming processes. Two types of fold terminations are considered here; "Periclines" (Price and Cosgrove (1990)) and conical folds (Dahlstrom (1954); Evans (1963); Stauffer (1964); Wilson (1967)).

1.1.3. Periclines Contending with Conical Folds. Periclines are elongate, doubly-plunging, domes (anticlines) or basins (synclines) that terminate at both ends of the fold. The term "conical folds" has its origin in π-diagrams of non-cylindrical folds being described by small circles, which traditionally are interpreted to correspond to portions of geometrical cones leading to the term "conical fold."

Conical folds, as a description for the shape of non-cylindrical folds, especially the terminus of folds, has gained wide acceptance as a special class of folds (Appendix A), such that *periclinal* folds have also been classified as *conical* (e.g., Evans (1963); Kelker and Langenberg (1982)).

1.2. RESEARCH OBJECTIVES

The concept of conical folds, while having limited practical usefulness (e.g., see Groshong, Jr., 2006), is a misleading visual representation of the actual shape of fold terminuses. To investigate shape changes near the terminus of folds, dynamic numerical

simulations (based on Liu *et al.* (2016)) and computer aided design (CAD) are utilized to create virtual periclines of varying aspect ratios. From these periclines synthetic stereograms, tangent-, SCAT-, and curvature plots are generated. Comparison of synthetic plots with plots from natural buckle folds in Missouri as well as examining geometric attributes of these folds suggests the *a priori* interpretation of π-diagrams with small circles as conical folds likely diminished the recognition of many natural folds terminate with a form compatible with periclines. Accurate geometric characterization of how folds end has consequences for dynamic modelling of how folds form; it is pointless to continue the misconception of conical folds if we are to advance in understanding fold forming processes.

2. METHODOLOGY

2.1. GENERAL PROCEDURE

Periclines are well known from field exposures (e.g., Dubey and Cobbold (1977); Nickelsen (1979); Nickelsen and Cotter (1983); Price and Cosgrove (1990); Sattarzadeh *et al.* (1999)) are readily produced in dynamic modelling (Fernandez and Kaus (2014); Liu *et al.* (2016)). For this study, virtual pericline surfaces, with aspect ratios of 1:10 and 1:3 (half wavelength to hinge length), extracted from numerical models of a single-layer 3D buckle fold (Liu *et al.* (2016)), are re-discretized using Altair HyperMesh™ to a high resolution (i.e., 1600 rectangular planar elements). This allows creation of high spatial resolution data sets of surface attitudes (strike and dip) along any orientation (profiles A, B, C, and D; Figures 2.1 and 2.2) to simulate data collected from natural folds along transects such as road-cuts, railroad-cuts, river-cuts, by geologists.

2.2. MATLAB™ SCRIPTS

A MATLAB™ script processes the point cloud and determines the attitude (strike and dip) of individual elements along the transect (Hasbargen (2012)). To utilize this script, the required input is a Microsoft Excel™ spreadsheet with the coordinates (x, y, z) in easting, northing, and elevation. Each "plane" will consist of one row in the spreadsheet and requires three coordinate points. This script will append separate arrays of strike, dip, and dip direction (right-hand rule) to a new worksheet in the spreadsheet and will create a .txt file with the information. A second MATLAB™ script accepts a Microsoft Excel™ spreadsheet as an input, with the first column being the dip, and the second the dip direction (right-hand rule). It will output a figure with a tangent diagram (Bengtson (1980)). The MATLAB™ scripts are available in supplementary material.

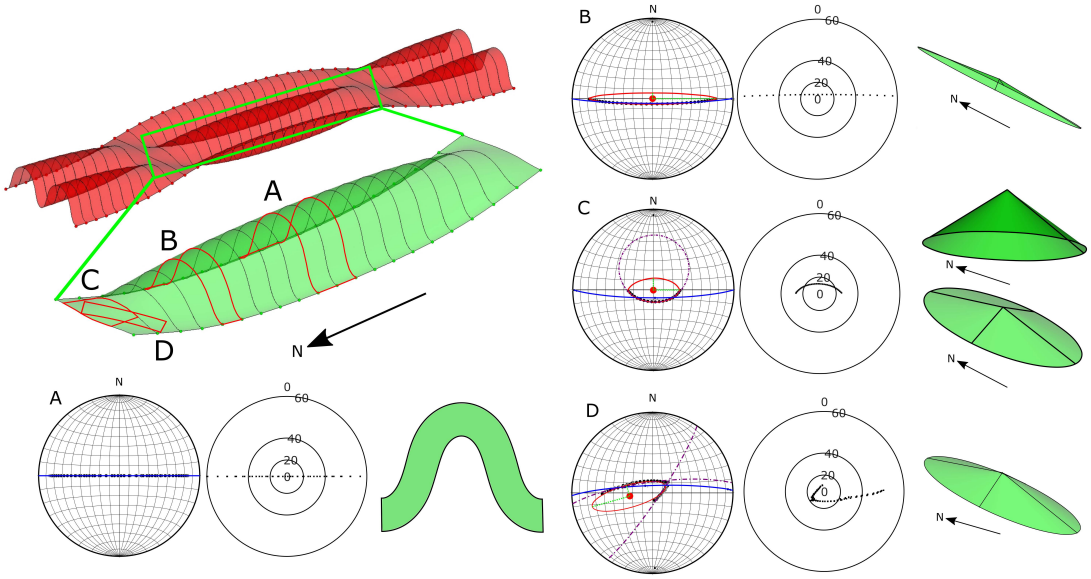

Figure 2.1. A single pericline with a 1:10 aspect ratio extracted for detailed structural analysis from a field of identical periclines generated by numerical modelling of buckle folding (Liu *et al.* (2016)). Orientation data from transects (red boxes) perpendicular (A, B, and C) and at 45° (D) to the longitudinal fold axis and corresponding stereographs and tangent diagrams with best fit great circle (blue), small circle (dotted), or ellipse (red) are shown. Green cylindrical and conical surfaces, reversed engineered from the corresponding stereogram patterns are shown slightly tilted for improved visibility.

π-diagrams, including optimal great-, and small-circle fits (Allmendinger *et al.* (2012); Cardozo and Allmendinger (2013)), and tangent diagrams (Bengtson (1980); Groshong, Jr. (2006)) are constructed for each transect. In addition, SCAT (Bengtson (1981); Groshong, Jr. (2006); see Appendix C) and 3D curvature analysis (Lisle (1994); Bergbauer and Pollard (2003), Mynatt *et al.* (2007); see Appendix C) of the entire pericline is also completed.

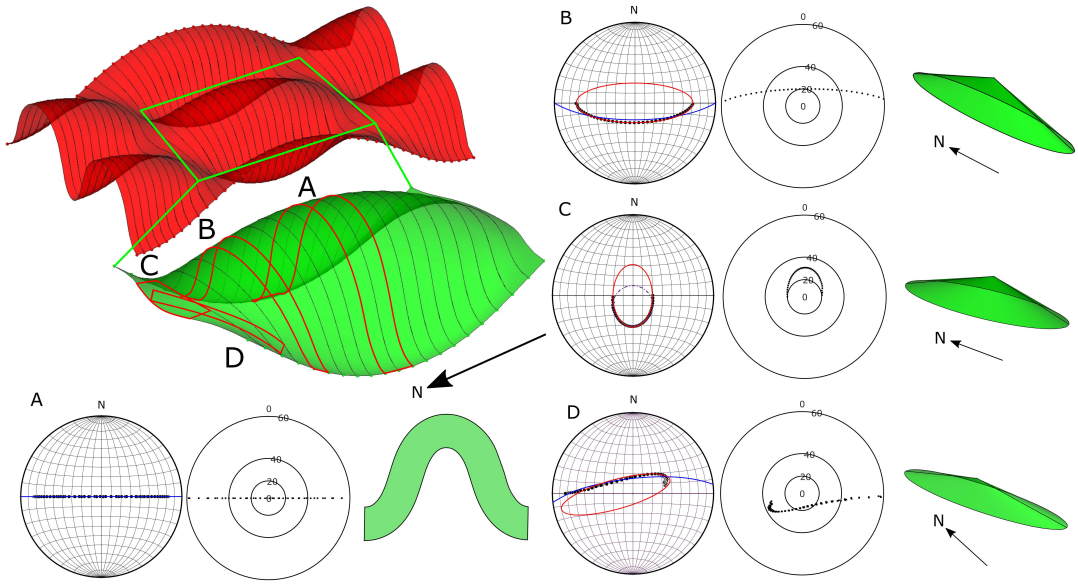

Figure 2.2. A single pericline with a 1:3 aspect ratio extracted for detailed structural analysis from a field of identical periclines generated by numerical modelling of buckle folding (Liu *et al.* (2016)). Orientation data from transects (red boxes) perpendicular (A, B, and C) and at 45° (D) to the longitudinal fold axis and corresponding stereographs and tangent diagrams with best fit great circle (blue), small circle (dotted), or ellipse (red) are shown. Green cylindrical and conical surfaces, reversed engineered from the corresponding stereogram patterns are shown slightly tilted for improved visibility.

3. RESULTS

3.1. VIRTUAL NON-CYLINDRICAL FOLDS

3.1.1. Perpendicular Cross-sections (Transects A, B, and C). Geometric analysis of the virtual periclines, using high spatial resolution strike and dip data extracted along several profile transects from the middle to the terminus of the folds, are shown as stereograms and tangent diagrams (Figure 2.1 and 2.2). The corresponding geometric cone shapes (shown in green), reverse engineered from either the π-diagrams or the tangent diagrams, have been inclined slightly from their steeply plunging cone axis (and *vertical* for the elliptical cones) for better perspective (Figures 2.1 and 2.2). Transect A across the center of the 1:10 and 1:3 periclines have a π-diagram described by great circles, representing the central cylindrical portion of the fold. The orientation of the axial surface is 000, 90° and the plunge and trend of the hinge line is 0°, 000 for periclines of both aspect ratios. Tangent diagrams confirm these are cylindrical folds as dip-vector orientation data define straight lines for cylindrical folds and hyperbola for conical folds (Bengtson (1980)). Transect B of the 10:1 pericline has an ambiguous π-diagram (e.g., see Bengtson (1980)) described by either a great circle or by an ellipse. If treated as a near-cylindrical fold the orientation of the axial surface is 000, 90° and plunge and trend of the hinge line is 5°, 180; an acceptable result for constraining the direction of closure. However, the tangent diagram for transect B unequivocally confirms this is a non-cylindrical fold (see Bengtson (1980); Groshong, Jr. (2006)). Conical folds do not have axial surfaces; the plunge and trend of the crest- (or trough) line of the fold is used to determine the orientation of the vertex of the cone (Groshong, Jr. (2006)). Transect C of the 1:10 pericline, close to the nose of the fold, has a π-diagram best described by either an ellipse or a small circle; a great circle, with an ~10° plunge to the north, is also shown. Small circles and ellipses are better developed for

transects B and C for periclines with the 1:3 aspect ratio (Figure 2.2). Folds with π-diagrams described by small circles traditionally are classified as conical folds (e.g., Bucher (1944); Dahlstrom (1954); Bengtson (1980); Twiss and Moores (1992); Lisle and Leyshon (2004); Groshong, Jr. (2006); Davis *et al.* (2011) see Appendix B).

3.1.2. 45° Cross-sections (Transect D) and the "Fish-hook" Pattern. Profile sections are used for characterizing the true shape of folds (e.g., Ramsay (1967)). However, for many folds, orientation data collected over a broader area is plotted on a π-diagram to characterize the shape of the fold. Transect D of the 1:10 and 1:3 periclines, which traverses the folds at 45° to the fold axis near the terminus of the folds, yields a "fish-hook" stereogram and tangent diagram best fit by an ellipse rather than a great- or small-circle (Figures 2.1D and 2.2D).

A less robust, poorly exposed, data set from this same area of a natural, but similar to the 1:10 pericline might allow for a π-circle fit with an orientation of 088, 90° with a hinge line oriented 8°, 178. If either one side or the other of the "fish-hook" pattern was present, two very different π-circles are possible. The first π-circle defines an axial plane with an orientation of 262.5, 78.6° and a hinge line of 11.4°, 172.5 and the second defines an axial plane with an orientation of 034, 82.6° and a hinge line of 7.4°, 304. In a poorly exposed field of folds, the possibility of disparate π-circles suggest irregular folding even though the actual folds are highly regular (Figure 2.1).

3.2. NATURAL NON-CYLINDRICAL FOLDS

Natural folds with ambiguous to complex π-diagrams, similar to the synthetic patterns for the virtual periclines (Figures 2.1 and 2.2), are present in the Ozark Plateau of south-central Missouri (Figure 3.1) (Liu (2016)). Here, a series of buckle folds in sandstones of the lower Ordovician Roubidoux Formation are discontinuously exposed for over seven kilometers in road cuts along US Highway 63, near Licking, Missouri. Highway 63 defines a ~30° oblique transect across the longitudinal fold axes of these folds (Figure

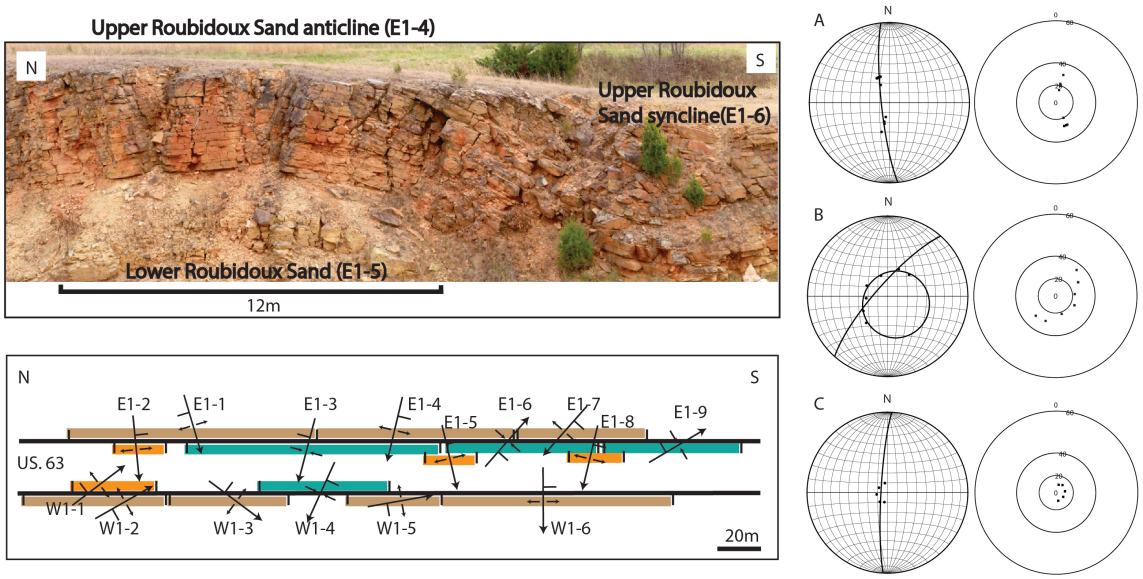

Figure 3.1. Periclinal buckle folds in Missouri (Liu (2016)). Great circle interpretation (left stereonet) and conical interpretations (right stereonet) of fold attitude data plotted below each pictured field site.

3.1). π-diagrams of bedding orientation data from multiple folds exposed along the high-way define rare great circles, small circles, and ellipses with “fish-hook” patterns (Figure 3.1). These anticlinal and synclinal fold axes exhibit common orientations commonly and opposing plunge directions over short distances (Figure 3.1). Folds with axial surfaces discordant to the general trend are rare.

4. DISCUSSION

4.1. VISUALIZATION OF FOLD SHAPE INTERPRETATIONS

The following "traditional" interpretations for the folds exposed along Highway 63 could be made:

1. π-diagrams fit by great circles are "cylindrical" to near-cylindrical folds.

2. π-diagrams that define small circles are "conical" folds of different sizes with near vertical cone axes.

3. Folds that exhibit "fish-hook" patterns are enigmatic as elliptical circles are currently unavailable as a possible fit using software for stereographic analysis (e.g., see Stereonet 10).

It is likely that such fish-hook patterns would be interpreted as either near- or a non-cylindrical "elliptical" conical folds based upon the extent to which the poles to the planes scatter around a great circle or a small circle "fit". Utilizing π-diagrams, geometric analysis of folded Roubidoux formation sandstone would indicate they are complex shapes consisting of multiple non-cylindrical "conical" folds and rare cylindrical to near cylindrical folds. These anticlinal and synclinal folds change plunge commonly exhibit opposing plunge directions over short distances (Figure 3.1) and create the impression of a basin and dome fold interference pattern (see Ramsay and Huber (1987)).

While conical surfaces are a permissible mathematical solution to patterns displayed in stereograms or tangent diagrams, the strong similarity of the synthetic diagrams obtained from the virtual pericline (a non-conical fold shape) compared to the reverse engineered cones (Figure 2.1) indicates that π- and tangent diagrams simultaneously allow for two possible fold geometry solutions. One is more realistic (pericline) and the other more

imaginary (conical). The failings of cones to accurately represent the true geometrical shape of folds, especially fold terminuses, can be demonstrated through comparative visualization of the pericline and conical surfaces and quantification of changes in fold shape along the hinge \crestal line in the fold plunge direction.

The virtual 1:10 pericline and the elliptical cone reverse engineered from the small-circle solution to the π-diagram for transect C (Figure 2.1), are shown together for comparison (Figure 4.1). The elliptical cone, with its vertical cone axis, exhibits limited surface overlap (<10%) over a spatially restricted portion near the terminus of the pericline (Figure 4.1). A domain approach (see Nicol (1993)) utilizing many multiple cones, of varying sizes, in similar upright orientations, spatially spread along the hinge\crestal line is still unlikely to fully describe the pericline surface.

Non-cylindrical folds with π-diagrams that define small circles, that are interpreted as conical folds with near vertical cone axes and downward opening cones, are common (e.g., see Webb and Lawrence (1986); Becker (1995); Mandujano V and Keppie M (2006); Pastor-Galán *et al.* (2012)). However, this orientation for cones may seem counter-intuitive as the type diagram for conical folds (e.g., Bengtson (1980)) shows the cone vertexes to be gently to moderately plunging (<30°). The crestal line of the conical fold plunging ~15°either away from the cone vertex (Type I) or towards the cone vertex (type II). These cones are a permissible solution to the folds shown in Bengtson (1980) which have steeply dipping to vertical limbs. For comparative purposes, we show recumbent cones and elliptical cones with profile sections that match profile sections of the pericline (Fig. 3). The vertices of each cone is constrained to coincide with the pericline terminus. It is important to note that the recumbent cones are not a rigorous permissible solution to the π- or tangent-diagrams generated for the pericline. The orientation (plunge and trend) of the crest-line for the recumbent cones is concordant to the pericline. However, the shape of the recumbent cones are a poor description of the folded surface of the pericline. Again, it is unlikely that multiple recumbent conical- to elliptical folds would can fully describe the pericline.

Similarly, Bengtson (1980) highlights only a small portion of the presumably topographic surface of the fold that coincides with the cone; the shape of the terminus of the fold(s) as the vertex of the cone(s) is approached is not shown.

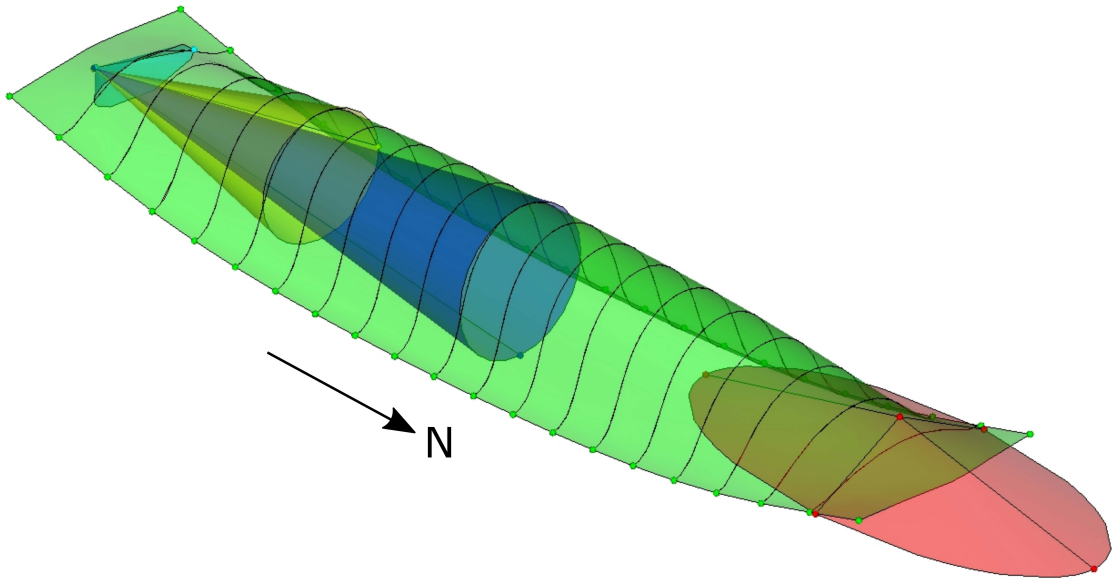

Figure 4.1. Engineering cones to approximate a "fit" to the virtual pericline. The reverse engineered cones fit the pericline surface at the cone base only to the south of the diagram. The vertical axis cone "fits" the tip of pericline at the northern edge.

4.2. QUANTITATIVE DISTINCTIONS OF CONICAL FROM PERICLINAL FOLD SHAPES

Visual comparison of cones reverse engineered from the synthetic π- and tangent diagrams and that of actual pericline surface qualitatively illustrate the shape of the terminus of conical folds and periclines are fundamentally different (Figure 4.1). For extremely well exposed natural folds, folded surfaces can be captured as point clouds (e.g. Sheep Mountain anticline, see Mynatt *et al.* (2007)) and analyzed using curvature analysis (e.g., Midland Valley's Move™ 2017.2 software for SCAT, 3D curvature, and differential geometry analysis) to classify the fold (Bergbauer and Pollard (2003); Lisle and Toimil (2007); Mynatt *et al.* (2007)). The 3D curvature analysis of the virtual pericline (see Appendix C)

confirms a periclinal geometry and does not indicate a Gaussian curvature of 0 (indicative of a cone) consistently across the structure. More commonly, natural folds are incompletely exposed precluding application of these comprehensive surface analysis techniques. In such cases, distinguishing conical folds from periclines can be quantitatively demonstrated by comparison of the change in the ratio of the fold amplitude (A) to the fold width (W) or half-wavelength (λ\2) along the hinge\crestal line in the direction of the plunge of the fold (Figure 4.2).

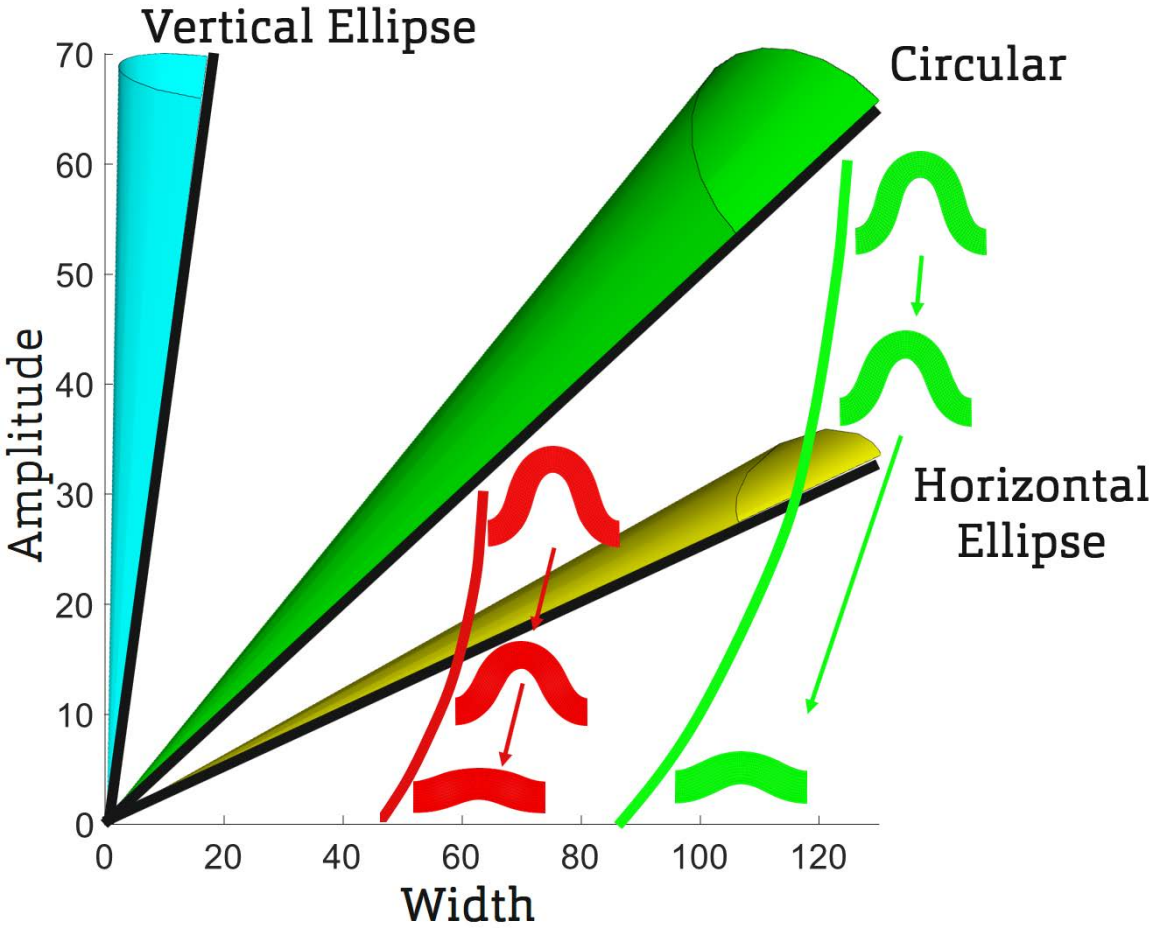

Figure 4.2. Plot of amplitude over half wavelength of virtual folds and various common shapes.

For a circular conical fold A\W = 1\2 and remains constant along the length of the crestal-line to the termination of the conical fold at the origin (Figure 4.2). For elliptic cones A\W is also a constant reflecting both the orientation and ratio of the major and minor axes of the ellipse (Figure 4.2). Profile sections of cylindrical to near-cylindrical folds of different sizes by definition also plot along these trend lines (e.g., see Fig. 15.27 of Ramsay and Huber (1987)). However, profile sections along the crestal line of the same fold, from the center to the terminus, will follow these trend lines to the origin if the fold is conical. In contrast, the A\W ratio of profile sections of periclines varies along the crestal line in the direction of the plunge of the fold. Near the center of the pericline, the shape of the folded surface is cylindrical and can be locally, partially approximated by elliptical cones of vary aspect ratios, at different locations along the crestal line (Figures Figure 2.1 and Figure 4.1). Thus, the trend line defined by the sequence of profile sections along the pericline crestal line cuts sharply across the linear trend lines of the circular to elliptical cones and does not terminate at the origin (Figure 4.2). The location of the starting point of the trend line is dictated by the size of the pericline. Similarly, distinguishing conical folds from periclines can be determined from the variation in the dip (plunge) along the trend of the crestal-line from the center to the terminus of the fold (Figure 4.3).

Conical folds will maintain a constant dip (plunge) along the length of the crestal line that reflects a combination of the orientation of the vertex and the aspect ratio of elliptical cones. In contrast, the variation in the dip (plunge) along the trend of the crestal-line from the center to the terminus of the periclines varies (Figure 4.3). The shape of the trend line reflects the profile and aspect ratio of the pericline.

4.3. REALISTIC RHEOLOGICAL MODELS REQUIRE ACCURATE FOLD SHAPES

Although numerous formation mechanisms have been proposed for conical folds (e.g., Ross (1962); Rickard (1963); Stauffer (1964); Becker (1995); Harris *et al.* (2002); Pastor-Galán *et al.* (2012)), all of them require specialized conditions of a locally non-

uniform horizontal strain field. True conical folds where the apex of the fold terminates at a singularity are difficult to reproduce using dynamic analysis. In contrast, periclines form within a locally uniform horizontal strain field in a simple deformation event (e.g., Fernandez and Kaus (2014); Liu *et al.* (2016)). The field of periclines, produced by finite-element models, utilizing realistic relationships among force, stress, mechanical strength properties, and strain (e.g., Figure 2.1), mimic closely natural buckle fold interference manifestations and fold terminations (e.g., Figure 3.1). While schematic representations of conical folds are common (e.g. Wilson (1967); Systra and Skornyakova (1980); Webb and Lawrence (1986); Nicol (1993); Becker (1995); Keppie *et al.* (2001); Pueyo *et al.* (2003); C. *et al.* (2005); Mandujano V and Keppie M (2006); Pastor-Galán *et al.* (2012)) the validity of natural folds terminating at a point can be readily evaluated from trend lines defined by readily measurable fold characteristics along the crest-line of the fold in the direction of the plunge (Figure 4.3).

4.4. THE POPULARITY OF PERICLINES

Periclines and conical folds have intrinsically distinct geometries while exhibiting similar patterns on π-diagrams. Why then has "conical fold" achieved elevated status as a special class of folds whereas periclines are rarely mentioned (see Appendix A)? Geometric analysis of the virtual pericline indicates a high probability for π-diagrams exhibiting equivocal patterns, ones that can be fitted by either great-circles or small-circles, as well as those fitted by small circles or ellipses (Figure 2.1). In contrast to great-circles, fitting small-circles to bedding orientation data with analog stereonets requires considerably more steps (e.g., see Billings (1972); Lisle and Leyshon (2004)); a task now readily completed using sophisticated software packages for stereographic analysis (e.g., Stereonet 10). This, and the *a priori* interpretation that the shape of folds that have π-diagrams described by small circles must be cones and therefore are conical folds, suggests a likelihood that π-diagrams

of natural periclines (see Figures 2.1 & 3.1) have been misclassified as conical folds. For example, based upon the π-diagrams alone, the folded sandstones in the Roubidoux Formation previously would be interpreted as conical folds rather than as periclines.

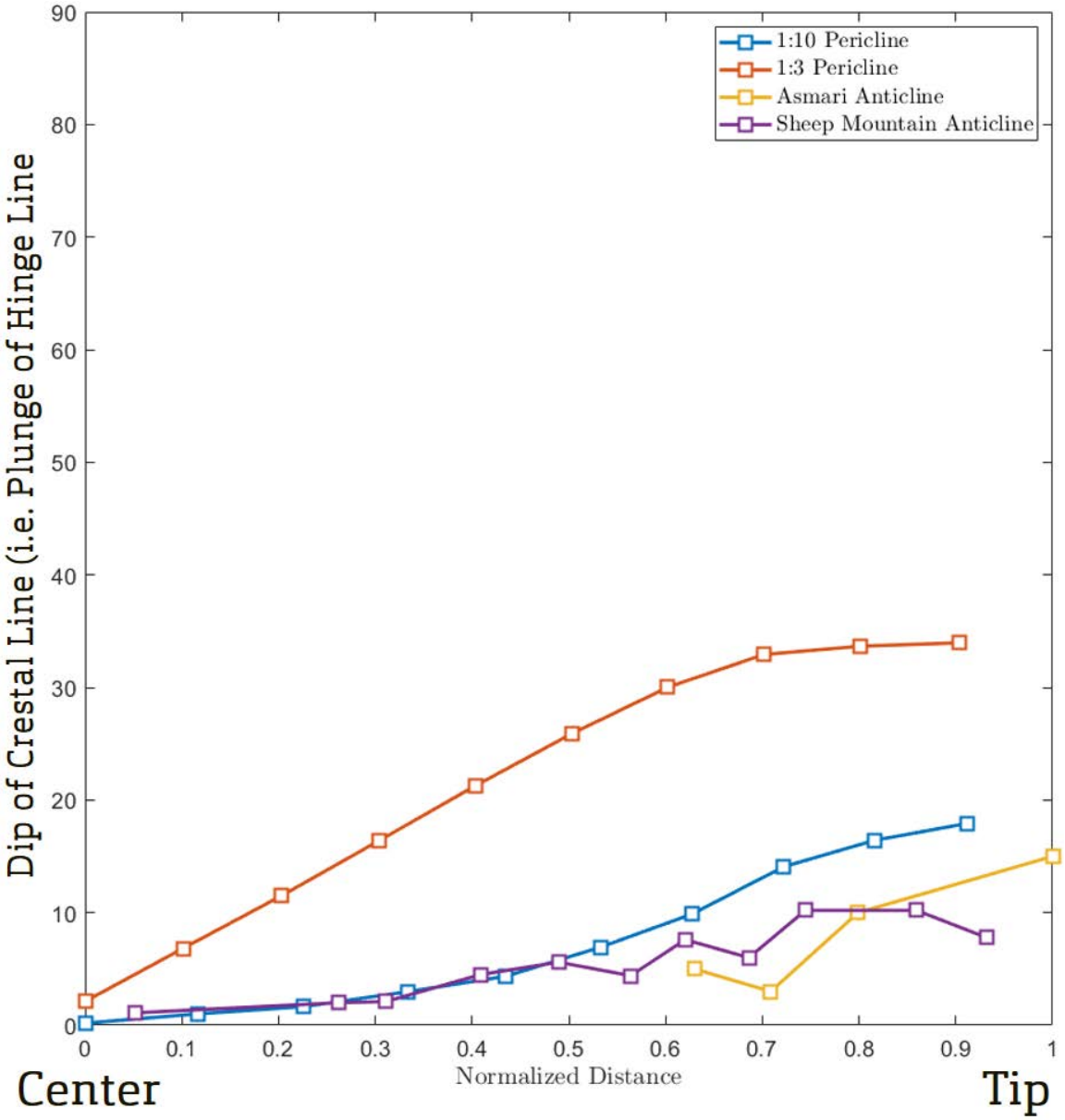

Figure 4.3. Plot of crestal line dip along normalized distance from the assumed cylindrical section (middle of fold) to the tip (Banerjee and Mitra (2004); Khodabakhshnezhad *et al.* (2015)).

5. CONCLUSIONS

While a conical surface is a mathematically permissible solution, as well as the traditional interpretation, for small-circles on π-diagrams, heed caution as cones are an inadequate and misleading representation of the true geometrical form of natural fold shapes – especially periclines. Conical folds, if they exist, must terminate at a point; this requires the A/W of the fold and the plunge to remain constant along the entire length of the crestal-line to the terminus of the fold. In contrast, periclines terminate by gradual dissipation of the fold, as shown by the decrease in A/W the plunge along the crestal-line of the fold. Pericline fold shapes are readily reproduced by dynamic modelling using realistic relationships among force, stress, strain, and the mechanical strength properties of rocks in a single uniform deformation event. Natural examples of periclines are common throughout the world including the Zagros Mountains in Iran (Price and Cosgrove (1990); Sattarzadeh *et al.* (1999)), the "Whaleback" pericline in Bude, North Cornwall, England (Dubey and Cobbold (1977)), and the "Whaleback" pericline in the Bear Valley Strip Mine in Shamokin, Pennsylvania, United States (Nickelsen (1979); Nickelsen and Cotter (1983)). The presented results suggest reliance on π-diagrams and tangent diagrams alone has led to misclassification of periclines and overrepresentation of conical folds. Consequently, conical folds may have not gained elevated status if visual comparisons between natural fold surfaces and corresponding conical-fold shapes compatible with π-diagrams were available (i.e., Figures 2.1 & 4.1). The ability to utilize virtual fold surfaces to create and analyze synthetic orientation data sets (e.g., π-diagrams) allows geologists to better visualize and interpret the results of natural data sets. It is confirmed that, if available, 3D curvature data is necessary to describe the true 3D geometry of a fold (see Appendix C). Similarly, evaluation of variation in A\W and plunge along the trend of folds readily distinguishes between conical and periclinal folds. In order to advance our geometric, kinematic, and

dynamic understanding of fold formation, cones are pointless as descriptors of natural fold and the attention of the current and future geologists studying folds needs to be redirected towards characterizing and understanding more realistic fold shapes such as periclines.

APPENDIX A.

INTRODUCTION TO PERICLINES AND CONES

1. PERICLINAL FOLDS

Periclines are anticlines or synclines that form domes and basins, incorporating a doubly-plunging hinge line (Figure 1) (Price and Cosgrove (1990)). Periclinal folds are commonly characterized by using their aspect ratio: half wavelength to hinge length, illustrated in Figure 1 (Cosgrove and Ameen (1999)). These folds form as a result of fold interference patterns of buckling (Price and Cosgrove (1990)), and can be caused by a uniform horizontal strain field (e.g. Fernandez and Kaus (2014); Liu *et al.* (2016)). Some examples of natural periclines are the Zagros Mountains, Iran (Price and Cosgrove (1990), Sattarzadeh *et al.* (1999)), the “Whaleback” pericline in Bude, North Cornwall, England (Dubey and Cobbold (1977)), and the “Whaleback” pericline in the Bear Valley Strip Mine, in Shamokin, Pennsylvania, United States (Nickelsen (1979); Nickelsen and Cotter (1983)).

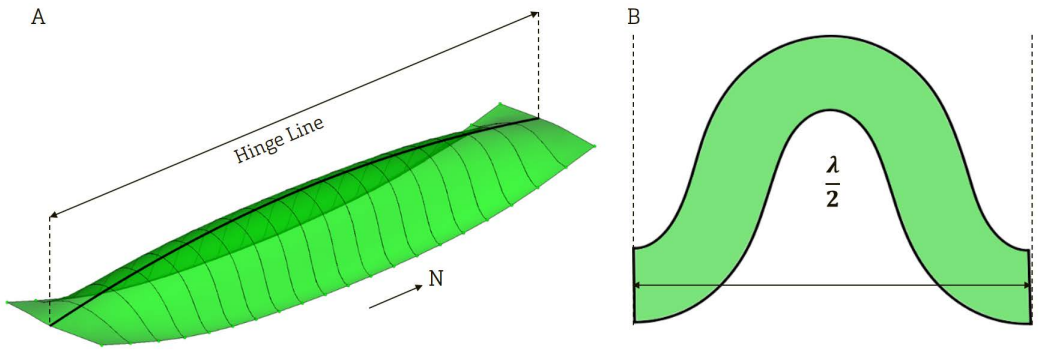

Figure 1. Virtual Periclinal fold generated by numerical simulation (Liu *et al.* (2016)). A illustrates the curved hinge line and B shows the cylindrical section (middle) fold profile.

2. CONICAL FOLDS

2.1. CONICAL FOLDS IN LITERATURE

Even though Ramsay (1967) (p. 349) and Ramsay and Huber (1987) (p. 311) state that "structures of this type are very rare" and "generally, layer morphology is more complex than that of a truly mathematical conical shape," a survey of the relevant literature shows

that conical folds seem to be frequently observed and documented in a variety of structural settings globally (Stauffer (1964); Wilson (1967); Stockmal and Spang (1982); Webb and Lawrence (1986); Kelker and Langenberg (1987); Kelker and Langenberg (1988); Nicol (1993); Becker (1995); Keppie *et al.* (2001); C. *et al.* (2005); Braid and Murphy (2005); Mandujano V and Keppie M (2006); Pastor-Galán *et al.* (2012); Mulchrone *et al.* (2013)). There are many formation mechanisms proposed for conical folds (see Discussion section).

Conical folds have been used to describe three-dimensional fold terminations of cylindrical folds as "vertical" cones with the apex adjacent to the fold hinge line (Webb and Lawrence (1986)), as "horizontal" cones with the apex along the axial trace (Keppie *et al.* (2001)), and further as "elliptical" cones versus "circular" cones (Haman (1961)). In addition, Nicol (1993) describes conical folds as part of dome and basin fold interference patterns.

2.2. GEOMETRY

A geologic fold termed a conical fold implies that the fold shape is at least part of a geometric cone and that the fold terminates. The surface is defined by a generatrix, which is a line that traces over the surface while being fixed at the vertex of the cone, shown in figure 2 (Groshong, Jr. (2006)).

A defining characteristic of a conical fold is the half-apical angle, which is the angle between the cone center-line axis through the center of the cone and the generatrix (Twiss and Moores (1992); Davis *et al.* (2011)). One way to describe the orientation of a cone is by the trend and plunge of the fold's center-line axis (Davis *et al.* (2011)). Conical folds can be identified on a stereonet by examining the π-diagram of the fold. If the π- diagram lies on a small circle, the fold is said to be conical (Twiss and Moores (1992)). The center of the small circle corresponds to the center-line axis of the conical fold, and the radius of the circle is 90° minus the half-apical angle of the cone (Twiss and Moores (1992)). Bengtson

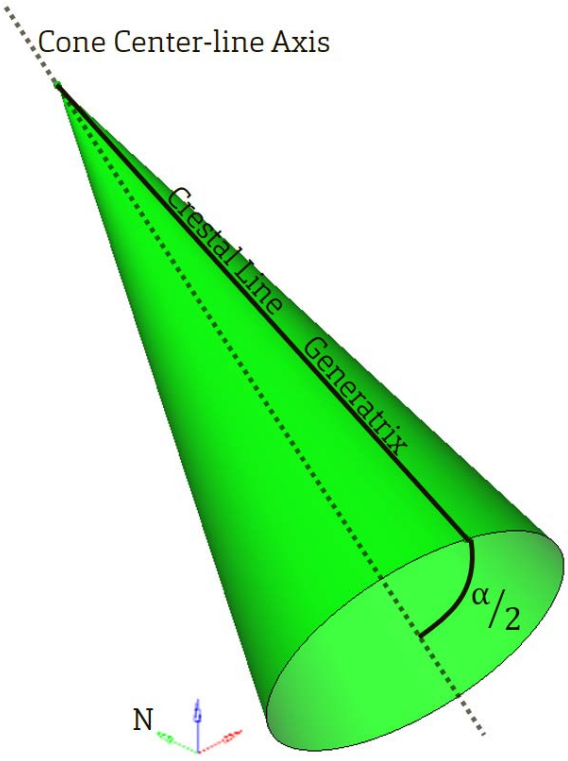

Figure 2. Geometry of a cone with geometric descriptors labelled.

(1980) describes the orientation of cones by the plunge of the crestal line, organizing cones into type I cones, where the vertex lies up-plunge, and type II cones, where the vertex lies down-plunge.

APPENDIX B.

GRAPHICAL CALCULATOR ANALYSIS

1. STEREONETS

Stereographic projection in the field of structural geology is, without a doubt, one of the most important tools. The adoption of stereographic projection arose as a need for thinking in three-dimensions and understanding spatial relationships. Bucher (1944) details the many different problems that can be approached by stereographic projection and helped show that stereonets are well-suited and practical tools. Soon after, Phillips (1960) presents a comprehensive resource on the strategies and application of stereonets, which highlights the growth of popularity and usefulness of the stereonet.

1.1. APPLICABILITY OF STEREONETS

Davis *et al.* (2011) crafts a practical guide to stereonet use in the field, describing how to perform various useful field calculations including (but not limited to):

1. Finding the orientation of lines and planes
2. Calculating the angle between lines or planes
3. Calculating the intersection orientation between two planes
4. Finding true dip from two apparent dips
5. Finding the angle between cleavage and bedding
6. Identifying and evaluating preferred orientations

Further information about defining the orientations of lines and planes and obtaining poles to planes can be found in Groshong, Jr. (2006), Davis *et al.* (2011), and many other major structural geology textbooks.

1.2. EQUAL-AREA AND EQUAL-ANGLE STEREONETS

The Schmidt net (equal-area net) is recognized as the preferred stereonet to use in structural geology over the Wulff net (equal-angle net) as an equal-area net is necessary for finding preferred orientations and contouring density distributions (Davis *et al.* (2011)). However, the Wulff net has the advantage of retaining angular relationships, which is advantageous for analysis of small circles (Lisle and Leyshon, 2004; Groshong, Jr. (2006)).

1.3. IDENTIFYING CONES WITH STEREONETS

1.3.1. π-diagrams. A convenient way to find the orientation of the fold axis using attitude data and a stereonet is the π-diagram. When poles to planes of a fold are plotted on a stereonet, the best fit great circle between them describes the orientation of a plane normal to the fold axis (Ramsay (1967)). The pole to the π-circle describes the orientation of the fold axis.

1.3.2. Disseminating Conical Fold Information from a Stereonet. A fold with a π-diagram with points that lie on a small circle on a stereonet is said to be a circular conical fold (see purple dashed circle in Figure 2.1) (Twiss and Moores (1992); Davis *et al.* (2011)). An elliptical conical fold can be identified as a fold with a π-diagram that lies in an ellipse (see Figures 2.1 and 2.2) and will have distinct short and long axes (Haman (1961)). The center of the small circle is the center-line axis of the conical fold; the radius of the small circle is equal to 90° minus the half-apical angle of the cone (Twiss and Moores (1992)). The values of half-apical angle and plunge and trend of the center-line axis are integral in constructing a synthetic cone. A small circle fit can be generated in programs similar to Stereonet 10 (Allmendinger *et al.* (2012); Cardozo and Allmendinger (2013)), or can be drawn by hand using an equal angle net that preserves the shape of a circle on the projection.

2. TANGENT DIAGRAMS

Another field plotting tool at the disposal of a structural geologist is a tangent plot, a way to represent field attitude data as vectors. They are also recognized as a convenient approach in determining whether a fold is cylindrical or slightly conical, amongst other applications (Bengtson (1980), Groshong, Jr. (2006)).

2.1. ANATOMY OF A TANGENT DIAGRAM

Tangent diagrams are circular diagrams with dip direction measured around the circumference and the angle of dip read from the concentric circles, which are calculated as the tangent of the dip angle (see in Figure 2.1). For this reason, tangent diagrams are generally used in low dip settings, as the dip scale becomes enormous above 80° (Bengtson (1980)).

2.2. IDENTIFYING CONES WITH TANGENT DIAGRAMS

Bengtson (1980) defines two types of cones based upon the location of plunge of the cone's vertex. A type I cone has the vertex up-plunge and will open up and flatten down-plunge, whereas a type II cone has the vertex down-plunge where the fold is converging (Groshong, Jr. (2006)). While a cylindrical fold plots on a tangent diagram as a straight line, an ideal type I or type II cone is represented by a hyperbola on the tangent diagram, and the curve is concave towards the vertex of the cone (Groshong, Jr. (2006)). This makes it especially simple and quick to determine if a dataset is cylindrical or non-cylindrical. One way to distinguish between type I and type II cones is the direction of concavity of the curve: type I cones will have a hyperbola concave towards the center, and type II cones will have a hyperbola concave away from the center (Bengtson (1980)).

Finding the orientation of a cone with a tangent diagram gives a different measurement than that of a stereonet. A vector drawn from the origin to the closest part of the curve will reveal the orientation of the crest or trough (Bengtson (1980)).

APPENDIX C.

SCAT AND CURVATURE ANALYSES

1. STATISTICAL CURVATURE ANALYSIS TECHNIQUES (SCAT)

Bengtson (1981) presents SCAT as a way to determine the bulk curvature of a structure using dipmeter data. One of this technique's main strengths is the ability to extract meaningful structural data from noise (Groshong, Jr. (2006)). Using the patterns found in dip-azimuth scatter plots, folds can be classified into 7 different models of bulk surface curvature (Bengtson (1981)). Using the dip-azimuth plots, the mutually perpendicular transverse (line of greatest structural change) and longitudinal (line of least structural change) axes can be determined (denoted T- and L- directions) (Bengtson (1981)). The L-axis is parallel to the crest or trough line of a structure and is perpendicular to the T-axis. Descriptions of the dip-azimuth patterns and the geologic bulk curvature they define can be found in Bengtson (1981) and Groshong, Jr. (2006). For this study, of note are the plunging fold and doubly-plunging fold bulk curvature patterns.

1.1. SCAT AND CONICAL FOLDS

SCAT can be easily performed in Midland Valley's Move™ 2017.2 software. Figure 1A shows a standing cone, with a half-apical angle of 28° (cone center-line axis vertical) and the corresponding dip-azimuth plot generated. The dip-azimuth plot reveals a constant dip at all azimuths, consistent with a geometric circular cone's constant dip, but does not accurately describe the T- or L- axes, as a standing circular cone does not have a defined crestal or trough line, and is reflected in the tangent diagram for the standing circular cone.

1.1.1. Circular Cone Example. When the circular cone's center-line axis plunge and trend is changed to 0°, 000 (Figure 1B), the type II cone shows a dip-azimuth plot consistent with the plot for a plunging fold (Figure 1d) (Bengtson (1981)). The T- and L-axes can be derived from this plot, consistent with a tangent diagram analysis.

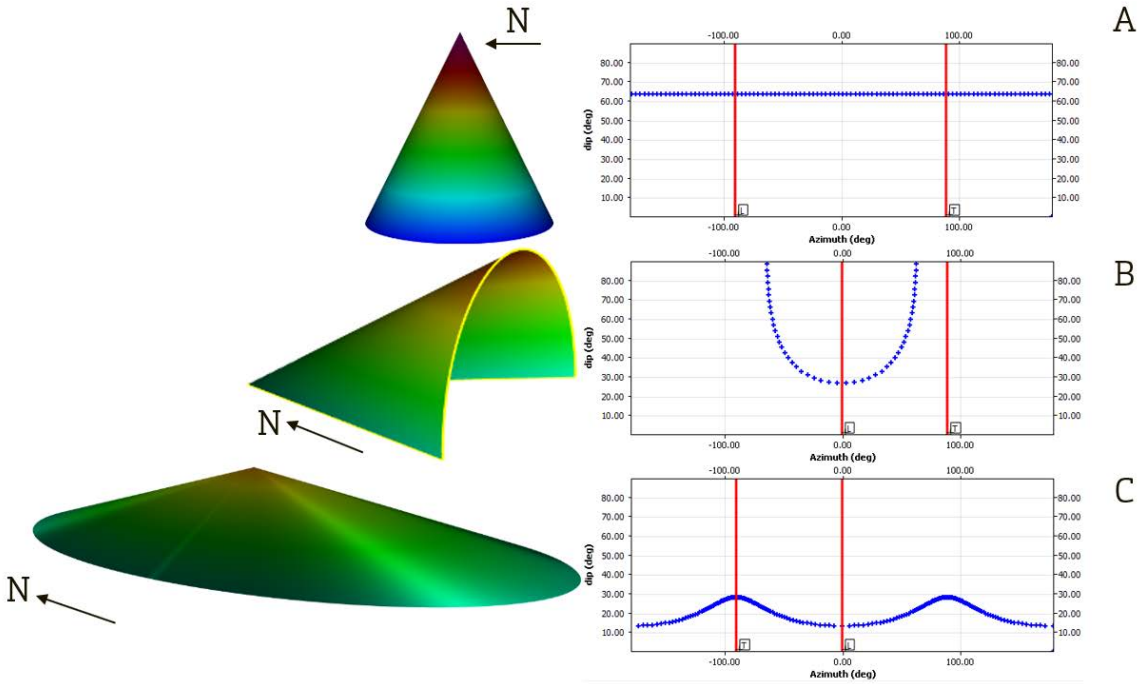

Figure 1. Comparison of results of application of SCAT to the (A) standing circular, (B) horizontal (type II), and (C) elliptical virtual cones.

1.1.2. Elliptical Cone Example. To demonstrate the difference between circular and elliptical cones with vertical center line-axes, an elliptical cone with a North-South half-apical angle of 62°and an East-West half-apical angle of 43° is created and analyzed with SCAT (Figure 1C). In this case, the dip-azimuth plot is similar in pattern to a doubly-plunging fold (e.g. Bengtson (1981)). There are definable T- and L- axes, as there is a discernible difference in the rate in structural change in perpendicular directions.

1.2. SCAT AND PERICLINES

Applying SCAT to the 1:10 and 1:3 pericline models produces similar results (Figure 2). Both periclines produce a dip-azimuth plot that matches the pattern of doubly-plunging folds (Bengtson (1981)). The peaks of the dip-azimuth plot of the 1:10 pericline have a "sharper" shape than the 1:3 pericline. The patterns of the dip-azimuth plots of periclines and cones are different as their surface curvature is different.

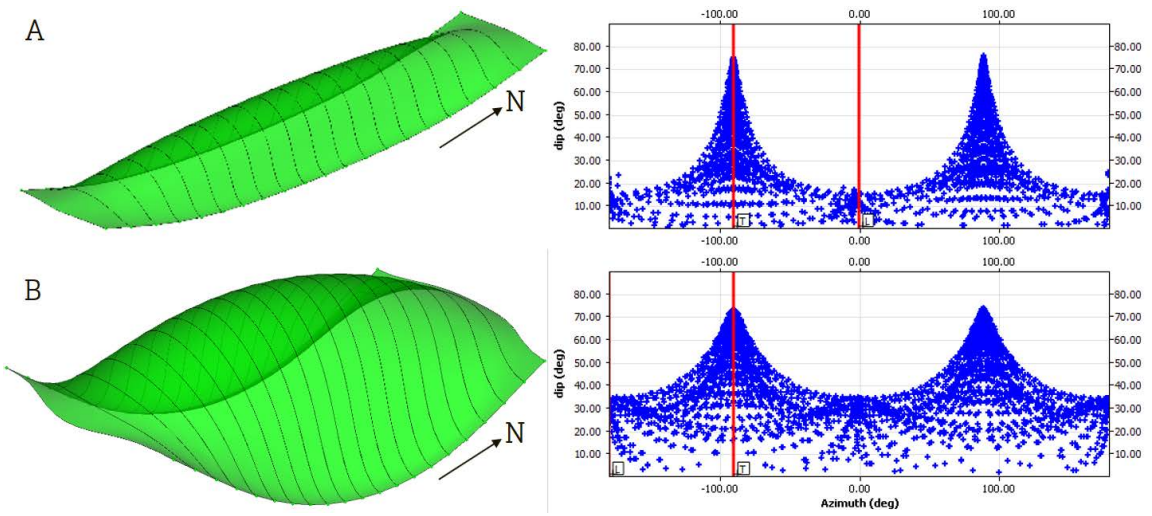

Figure 2. Comparison of results of application of SCAT to the (A) 1:10 and (B) 1:3 virtual periclines.

2. 3D CURVATURE ANALYSIS

2.1. 3D CURVATURE OVERVIEW

Differential geometry is used to characterize geological surfaces through calculating and observing the Gaussian and mean curvatures (Lisle and Toimil (2007); see Figure 2 in Mynatt *et al.* (2007); Zulauf *et al.* (2017)). Bergbauer and Pollard (2003) and Mynatt *et al.* (2007) provide derivations and further definitions of curvature, and a summary of the values of principal, mean, and Gaussian curvature are provided here. The values of mean and Gaussian curvature are found through calculating the principal curvatures of a surface, which represent the two orthogonal values of extreme normal curvature. Mean curvature is the arithmetic average of the two values of principal curvature and represents the orientation of a point of a surface (e.g. positive mean curvatures are antiformal structures or domes, negative mean curvatures signify synforms or basins, and zero mean curvatures are planar or can correspond to a perfect saddle, provided the Gaussian curvature is negative). Gaussian curvature is calculated in two ways: the product of the values of principal curvature or by angular deficit (Lisle (1994)). If the Gaussian curvature is zero, this signifies that one

principal curvature value must be zero and locally is cylindrically shaped. A positive Gaussian curvature corresponds to a dome or basin, whereas a negative value corresponds to a saddle.

2.2. DIFFERENTIAL GEOMETRY IN MIDLAND VALLEY'S MOVE™ 2017.2

Three-dimensional curvature analysis requires adequate exposure for the technique to be completely viable. Midland Valley's Move™ 2017.2 software can calculate the different values of curvature needed for differential geometry analysis. Mynatt *et al.* (2007) classification chart is used in the calculation of "geologic curvature" within Move™, extracting these values from a surface built in the software from a point cloud exported from computer-aided design software.

2.2.1. Differential Geometry Analysis of Circular and Elliptical Conical Folds. The mean, Gaussian, and "geological" curvature color maps of a vertically oriented elliptical cone (North-South half-apical angle of 62°, East-West half-apical angle of 43°) and a standing circular cone (half-apical angle of 28°) can be categorized within the Mynatt *et al.* (2007) table classification. The mean curvatures of the cones are positive values, while the Gaussian curvature is zero for both cones. The combination of these values results in a "geological" curvature of -2.5, which corresponds to a dome in Move™ 2017.2.

2.2.2. Differential Geometry Analysis of Periclines. Figure 3 contains the "geological" curvature color maps of the 1:3 and the 1:10 virtual periclines. The values of the mean and Gaussian curvatures are more complex in these structures. The "geologic" curvatures in these structures are very similar and cross through several different classifications possible in Move™ 2017.2. The surface curvatures of periclines and cones are distinctly different. Periclines are complex structures with varying surface curvature, changing the attributes of the surface. A conical fold, however, must retain one principal curvature value of zero, an inherent property of the surface, rendering the Gaussian curvature of a conical surface zero. Periclines and conical folds do not share the same surface geometry.

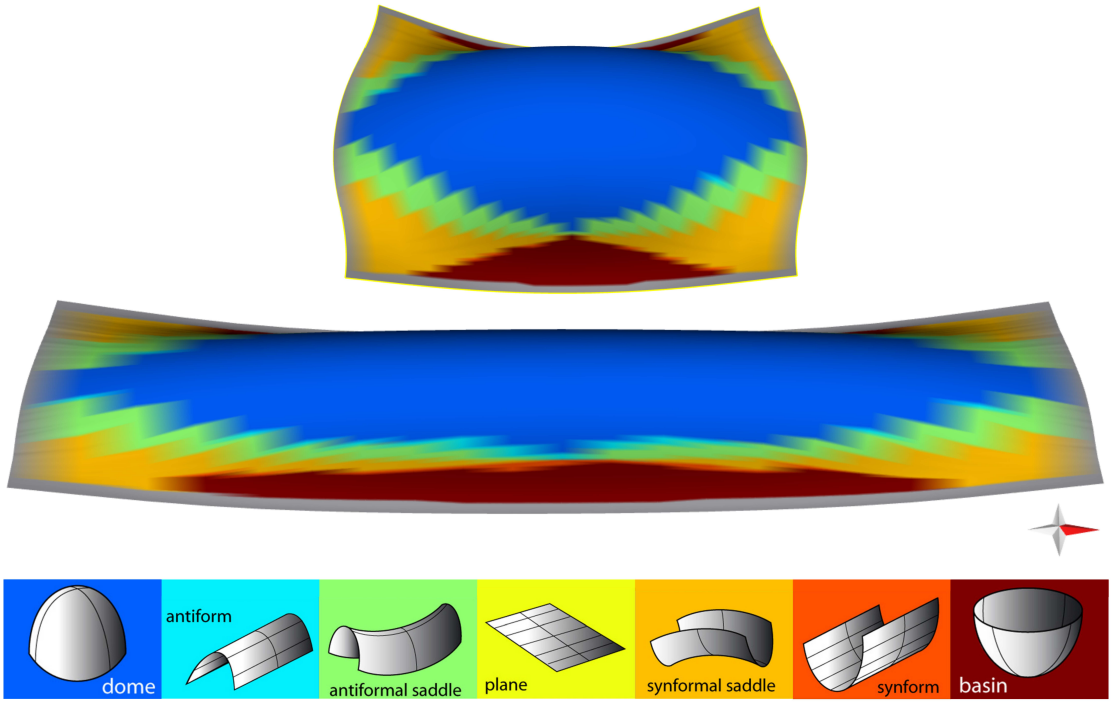

Figure 3. Geological curvature of the 1:3 (top) and 1:10 (bottom) virtual periclines calculated in Move™ 2017.2. Color scheme and categories from Mynatt *et al.* (2007).

REFERENCES

Allmendinger, R., Cardozo, N., and Fisher, D., *Structural geology algorithms: Vectors and tensors in structural geology*, Cambridge University Press, 2012.

Banerjee, S. and Mitra, S., 'Remote surface mapping using orthophotos and geologic maps draped over digital elevation models: Application to the sheep mountain anticline, wyoming,' American Association of Petroleum Geologists Bulletin, 2004, **88(9)**, pp. 1227–1237.

Becker, A., 'Conical drag folds as kinematic indicators for strike-slip fault motion,' Journal of Structural Geology, 1995, **17(11)**, pp. 1497–1506.

Bengtson, C., 'Structural uses of tangent diagrams,' Geology, 1980, **8(12)**, pp. 599–602.

Bengtson, C., 'Statistical curvature analysis techniques for structural interpretation of dip-meter data,' AAPG Bulletin, 1981, **65(2)**, pp. 312–332.

Bergbauer, S. and Pollard, D., 'How to calculate normal curvatures of sampled geological surfaces,' Journal of Structural Geology, 2003, **25(2)**, pp. 277–289.

Billings, M., *Structural Geology*, Prentice-Hall, Englewood Cliffs, New Jersey, 1972.

Biot, M., Odé, H., and Roever, W., 'Experimental verification of the theory of folding of stratified viscoelastic media,' Geological Society of America Bulletin, 1961, **72(11)**, pp. 1621–1631.

Braid, J. and Murphy, J., 'Acadian deformation in the shallow crust: an example from the siluro-devonian arisaig group, avalon terrane, mainland nova scotia,' Canadian Journal of Earth Sciences, 2005, **43(1)**, pp. 71–81.

Bucher, W., 'Studies for students: The stereographic projection, a handy tool for the practical geologist,' The Journal of Geology, 1944, **52(3)**, pp. 191–212.

C., E., Zille, A., and Rossi, G., 'The running-cone method for the interpretation of conical fold geometries: an example from the badia valley, northern dolomites (ne italy),' Journal of Structural Geology, 2005, **27(1)**, pp. 139–144.

Cardozo, N. and Allmendinger, R., 'Spherical projections with osxstereonet,' Computers & Geosciences, 2013, **51**, pp. 193–205.

Cosgrove, J. and Ameen, M., *Forced Folds and Fractures*, The Geological Society of London, London, 1999.

Dahlstrom, C., 'Statistical analysis of cylindrical folds,' Transactions of the Canadian Institute of Mining and Metallurgy, 1954, **57**, pp. 140–145.

Davis, G., Reynolds, S., and Kluth, C., *Structural Geology of Rocks and Regions, 3rd Edition*, John Wiley & Sons, Inc., Hoboken, New Jersey, 2011.

Dubey, A. and Cobbold, P., 'Noncylindrical flexural slip folds in nature and experiment,' Tectonophysics, 1977, **38(3-4)**, pp. 223–239.

Evans, A., 'Conical folding and oblique structures in charnwood forest, leicestershire,' Proceedings of the Yorkshire Geological Society, 1963, **34(1)**, pp. 461–492.

Fernandez, N. and Kaus, B., 'Fold interaction and wavelength selection in 3d models of multilayer detachment folding,' Tectonophysics, 2014, **632**, pp. 199–217.

Fleuty, M., 'The description of folds,' Proceedings of the Geologists' Association, 1964, **75(4)**, pp. 461–492.

Groshong, Jr., R., *3-D Structural Geology – A Practical Guide to Quantitative Surface and Subsurface Map Interpretation*, Springer-Verlag, Berlin Heidelberg, 2006.

Haman, P., *Manual of the Stereographic Projection for a geometric and kinematic analysis of folds and faults*, West Canadian Research Publications, Alberta, 1961.

Harris, L., Koyi, H., and Fossen, H., 'Mechanisms for folding of high-grade rocks in extensional tectonic settings,' Earth-Science Reviews, 2002, **59(1-4)**, pp. 163–210.

Hasbargen, L., 'A test of the three-point vector method to determine strike and dip utilizing digital aerial imagery and topography,' The Geological Society of America Special paper 492, 2012, pp. 199–208.

Hudleston, P., 'Fold morphology and some geometrical implications of theories of fold development,' Tectonophysics, 1973, **16(1-2)**, pp. 1–46.

Hudleston, P. and Lan, L., 'Information from fold shapes,' Journal of Structural Geology, 1993, **15(3-5)**, pp. 253–264.

Hudleston, P. and Lan, L., 'Rheological controls on the sahpes of single-layer folds,' Journal of Structural Geology, 1994, **16(7)**, pp. 1007–1021.

Hudleston, P. and Treagus, S., 'Information from folds: A review,' Journal of Structural Geology, 2010, **32(12)**, pp. 2042–2071.

Kelker, D. and Langenberg, C., 'A mathematical model for orientation data from macroscopic conical folds,' Mathematical Geology, 1982, **14(4)**, pp. 289–307.

Kelker, D. and Langenberg, C., 'A mathematical model for orientation data from macroscopic elliptical conical folds,' Mathematical Geology, 1987, **19(8)**, pp. 729–743.

Kelker, D. and Langenberg, C., 'Statistical classification of macroscopic folds as cylindrical, circular conical, or elliptical conical,' Mathematical Geology, 1988, **20(6)**, pp. 717–730.

Keppie, D., Keppie, J., and Murphy, J., 'Saddle reef auriferous veins in a conical fold termination (oldham anticline, meguma terrane, nova scotia, canada): reconciliation of structural and age data,' Canadian Journal of Earth Sciences, 2001, **39(1)**, pp. 53–63.

Khodabakhshnezhad, A., Arian, M., and Pourkemani, M., 'Folding mechanism in the asmari anticline, zagros, iran,' Open Journal of Geology, 2015, **5**, pp. 197–208.

Lisle, R., 'Detection of zones of abnormal strains in structures using gaussian curvature analysis,' AAPG Bulletin, 1994, **78(12)**, pp. 1811–1819.

Lisle, R. and Leyshon, P., *Stereographic Projection Techniques for Geologists and Civil Engineers, 2nd Edition*, Cambridge University Press, Cambridge, 2004.

Lisle, R. and Toimil, N., 'Defining folds on three-dimensional surfaces,' Geology, 2007, **35(6)**, pp. 519–522.

Liu, C., *Periclinal folding in Ozark Plateau: A record of local karst collapse or regional tectonic forces? [M.S. Thesis]*, Missouri University of Science and Technology, 2016.

Liu, X., Eckert, A., and Connolly, P., 'Stress evolution during 3d single-layer visco-elastic buckle folding: Implications for the initiation of fractures,' Tectonophysics, 2016, **679**, pp. 140–155.

Mandujano V, J. and Keppie M, J., 'Cylindrical and conical fold geometries in the cantarell structure, southern gulf of mexico: Implications for hydrocarbon exploration,' Journal of Petroleum Geology, 2006, **29(3)**, pp. 215–226.

Mulchrone, K., Pastor-Galán, D., and Gutiérrez-Alonso, G., 'Mathematica code for least-squares cone fitting and equal-area stereonet representation,' Computers & Geosciences, 2013, **54**, pp. 203–210.

Mynatt, I., Bergbauer, S., and Pollard, D., 'Using differential geometry to describe 3-d folds,' Journal of Structural Geology, 2007, **29(7)**, pp. 1256–1266.

Nickelsen, R., 'Sequence of structural stages of the alleghany orogeny, at the bear valley strip mine, shamokin, pennsylvania,' American Journal of Science, 1979, **279(3)**, pp. 225–271.

Nickelsen, R. and Cotter, E., 'Stop 3, bear valley strip mine, in nickelsen, r.p., and cotter e., eds., silurian depositional history and alleghanian deformation in the pennsylvania valley and ridge,' Annual Field Conference of Pennsylvania Geologists, 48th, Danville, PA, Guidebook, 1983, pp. 128–140.

Nicol, A., 'Conical folds produced by dome and basin fold interference and their application to determining strain: examples form north canterbury, new zealand,' Journal of Structural Geology, 1993, **15(6)**, pp. 785–792.

Pastor-Galán, D., Gutiérrez-Alonso, G., Mulchrone, K., and Huerta, P., 'Conical folding in the core of an orocline. a geometric analysis from the cantabrian arc (variscan belt of nw iberia),' Journal of Structural Geology, 2012, **29**, pp. 210–223.

Phillips, F., *The Use of Stereographic Projection in Structural Geology*, Edward Arnold (Publishers) Ltd., 1960.

Price, N. and Cosgrove, J., *Analysis of Geological Structures*, Cambridge University Press, United Kingdom, 1990.

Pueyo, E., Parés, J., Millán, H., and Pocoví, A., 'Conical folds and apparent rotations in paleomagnetism (a case study in the southern pyrenees),' Tectonophysics, 2003, **362(1-4)**, pp. 345–366.

Ramberg, H., 'Fluid dynamics of viscous buckling applicable to folding of layered rocks,' AAPG Bulletin, 1963, **47(3)**, pp. 484–505.

Ramsay, J., *Folding and Fracturing of Rocks*, McGraw-Hill, Inc., 1967.

Ramsay, J. and Huber, M., *The Techniques of Modern Structural Geology Volume 2: Folds and Fractures*, Academic Press Inc., London, 1987.

Rickard, M., 'Analysis of the strike swing at crockator mountain, co. donegal, eire,' Geological Magazine, 1963, **100(5)**, pp. 401–419.

Ross, J., 'The folding of angular unconformable sequences,' The Journal of Geology, 1962, **70(3)**, pp. 294–308.

Sattarzadeh, Y., Cosgrove, J., and Vita-Finzi, C., 'The interplay of faulting and folding during the evolution of the zagros deformation belt,' in J. Cosgrove and M. Ameen, editors, 'Forced Folds and Fractures,' pp. 187–196, Geological Society, London, Special Publication 169, 1999.

Schmalholz, S. and Podladchikov, Y., 'Strain and competence contrast estimation from fold shape,' Tectonophysics, 2001, **340(3-4)**, pp. 195–213.

Stauffer, M., 'The geometry of conical folds,' New Zealand Journal of Geology and Geophysics, 1964, **7(2)**, pp. 340–347.

Stockmal, G. and Spang, J., 'A method for the distincetion of circular conical from cylindrical folds,' Canadian Journal of Earth Sciences, 1982, **19(6)**, pp. 1101–1105.

Systra, Y. and Skornyakova, N., 'Conical folds in ancient complexly-folded metamorphic formations in northern karelia,' Geotectonics, 1980, **14(1)**, pp. 17–25.

Twiss, R. and Moores, E., *Structural Geology*, W. H. Freeman and Company, New York, 1992.

Webb, B. and Lawrence, D., 'Conical fold termination in the bannisdale slates of the english lake district,' Journal of Structural Geology, 1986, **8(1)**, pp. 79–86.

Wilson, G., ‘The geometry of cylindical and conical folds,’ Proceedings of the Geologists’ Association, 1967, **78(1)**, pp. 179–209.

Zulauf, G., Zulauf, J., and Maul, H., ‘Quantification of the geometrical parameters of non-cylindrical folds,’ Journal of Structural Geology, 2017, **100**, pp. 120–129.

VITA

Avery Joseph Welker is a native of Perryville, Missouri. In May 2013, he graduated from Perryville High School and simultaneously earned an associate's degree from the Missouri Academy of Science, Mathematics, and Computing at Northwest Missouri State University.

In May 2016, Avery received a Bachelor of Science degree in petroleum engineering from Missouri University of Science and Technology. As an undergraduate student, he was active in the residential life and within the petroleum engineering department communities on S&T's campus. After earning his bachelor's degree, he enrolled in the graduate program in petroleum engineering at S&T straightaway.

During his time as a graduate student, he took on several leadership roles, including a graduate teaching assistant for the mechanical earth modeling course for petroleum engineering majors, as the president of the National Residence Hall Honorary, graduate liaison for the Society of Petroleum Engineers and American Association of Drilling Engineers student chapters, and an intern with Devon Energy Corporation. He also served as the Student Representative to the University of Missouri Board of Curators.

Avery earned his Master of Science degree in Petroleum Engineering from Missouri University of Science and Technology in December 2018.